

http://pubs.acs.org/journal/aelccp

Influence of the Mechanism of Discharge Product Formation on the Electrochemical Performance and Cyclability of Aprotic Na-O₂ Batteries

Kunal Kalpesh Velinkar, Alex Von Gunten, Jeffrey Greeley,* and Eranda Nikolla*



Downloaded via UNIV OF MICHIGAN ANN ARBOR on December 29, 2023 at 19:57:56 (UTC). See https://pubs.acs.org/sharingguidelines for options on how to legitimately share published articles.

Cite This: ACS Energy Lett. 2023, 8, 4555–4562



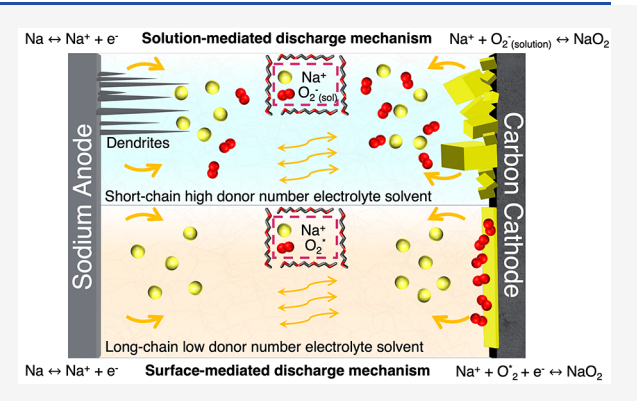
ACCESS

Metrics & More

Article Recommendations

Supporting Information

ABSTRACT: Na-O₂ batteries have emerged as potential alternatives to state-of-the-art lithium-ion batteries due to their high specific energy density. However, challenges related to poor overall efficiency and long-term stability have hindered their practical application. Understanding the deactivation mechanisms at the electrode/electrolyte interfaces is critical to overcoming these challenges. Herein, we investigate the effect of the cathode/electrolyte interface on the discharge mechanism by varying the glyme-ether electrolyte solvent and the nature of the carbon cathode. We report that discharge—charge energetics at carbon/electrolyte interfaces driven by surface-mediated discharge are sensitive to the nature of the carbon cathode. Their main deactivation mechanism involves the formation of undesired



discharged products, which can be mitigated by tuning the cathode surface. Conversely, discharge-charge energetics and deactivation of $Na-O_2$ cells driven by a solution-mediated discharge process have limited dependence on the carbon cathode. These findings have implications for effectively designing efficient and stable $Na-O_2$ batteries.

protic M-O₂ (M = Li/Na) batteries have gained significant attention as potential alternatives to commercial Li-ion batteries 1-6 due to their high theoretical energy densities and reversible redox chemistries. Among M-O₂ batteries, Li-O₂ systems have been the most studied because of their promising theoretical specific capacity.⁷⁻⁹ However, the large overpotential barrier required to dissociate the most thermodynamically stable discharge product, Li₂O₂, significantly increases the charge potential (>4 V vs Li/Li+), resulting in poor overall cell efficiency and stability. Alternatively, in Na-O2 systems, kinetics favor the one-electron-transfer reaction to form NaO2 over the twoelectron-transfer reaction to form Na2O2, leading to low overpotentials in the initial stage of charge. 10 Na is also more abundant than Li, making these systems more commercially attractive. Despite these advantages, Na-O2 batteries still face challenges related to their limited long-term stability.

The solvation properties of aprotic glyme-ether electrolyte solvents, described by their donor and acceptor numbers, have been shown to play a critical role in the discharge mechanism that governs the formation of $Na-O_2$ species at the cathode. These properties describe the ability of the

aprotic solvent to stabilize $Na^+-O_2^-$ ion pairs¹³ in the electrolyte. Specifically, the interaction of the aprotic solvent with the sodium salt in the electrolyte is influenced by the chain length of the solvent.¹¹ For instance, short-chain-length, high-donor-number (>18 kcal/mol) electrolyte solvents, such as diethylene glycol dimethyl ether (DEGDME), are reported to exhibit weak solvent—solute interactions with the sodium salt (NaOTF), resulting in an abundance of free solvent molecules. This consequently facilitates the stabilization of the $Na^+-O_2^-$ species in the electrolyte.¹¹ Subsequently, a quasiequilibrium state is established between the solvated $Na^+-O_2^-$ (sol) species in the electrolyte solvent and the adsorbed NaO_2^+ species on the cathode surface $(Na^+-O_2^-$ (sol) \rightleftharpoons NaO_2^+). Once a saturation limit of solvated species is

Received: August 11, 2023 Accepted: October 3, 2023 Published: October 9, 2023





ACS Energy Letters http://pubs.acs.org/journal/aelccp Letter

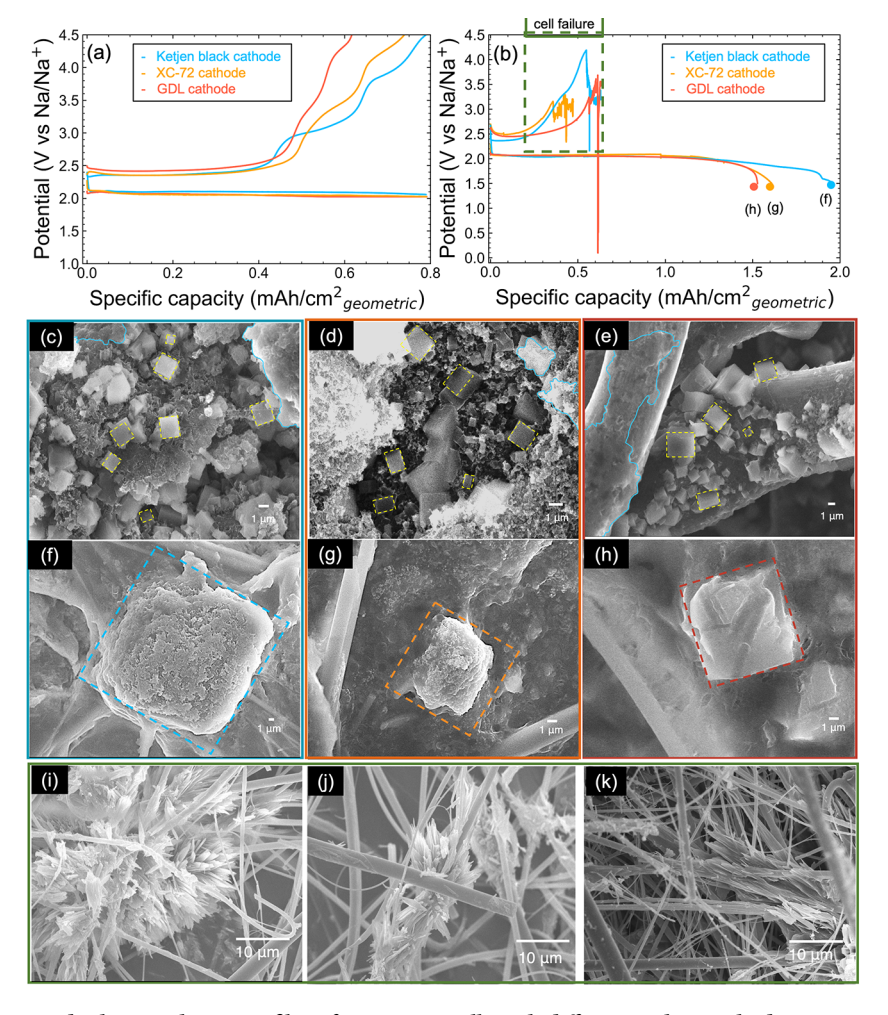


Figure 1. (a, b) Galvanostatic discharge—charge profiles of DEGDME cells with different carbon cathodes: Ketjen Black (K.B.) (blue), XC-72 (orange), and GDL (red), for a limited capacity of $0.79 \text{ mAh/cm}^2_{\text{geometric}}$ and full capacity, respectively, in a potential window of 1.5-4.5 V, at a current density of $80 \ \mu\text{A/cm}^2$. (c-e) SEM images post limited discharge for cells with K.B., XC-72, and GDL carbon cathodes, respectively (average size of $\sim 1.5 \ \mu\text{m}$ for all three cathodes). (f-h) SEM images post full discharge for cells with K.B., XC-72 (average size of $\sim 1.1 \ \mu\text{m}$), and GDL carbon cathodes (average size of $\sim 5 \ \mu\text{m}$), respectively. (i-k) SEM images of separator characterized when the cell undergoes fluctuations for K.B., XC-72, and GDL cathode cells, respectively.

achieved, the equilibrium shifts toward chemical deposition of solvated Na $^+$ –O $_2^-$ _(sol) species on the cathode surface, forming cubic-structured NaO $_2$ extended structures. Conversely, long-chain, low-donor-number solvents (<12 kcal/mol), ¹¹ such as tetraethylene glycol dimethyl ether (TEGDME), exhibit strong solvent—solute interactions with the sodium salt (NaOTF), leading to limited availability of free solvent molecules. This induces high barriers for solvation of Na $^+$ –O $_2^-$ species in the electrolyte, leading to surface-mediated discharge with limited contributions from the solution phase. ¹¹

The stability of Na–O $_2$ discharge products has been primarily studied for the DEGDME system, where their degradation is hypothesized to occur via multiple mechanisms. ^{14,15} For instance, it has been reported that cubic NaO $_2$ products undergo disproportionation, leading to the formation of (i) Na $_2$ O $_2$ ^{14,16} during discharge, and (ii) the hydrated peroxide (Na $_2$ O $_2$ ·2H $_2$ O) phase during idling. ¹⁵ Various strategies have been suggested to optimize solvent—solute interactions to limit the interaction between the solvated NaO $_2$ - species and the electrolyte solvent. One such approach involves reducing the concentration of free solvent molecules ^{17,18} in the electrolyte by increasing sodium salt

concentration.¹⁹ However, this leads to an increase in electrolyte viscosity²⁰ and a decrease in ionic conductivity, resulting in increased overpotential losses. In contrast, strategies to enhance stability by changing the electrolyte and promoting surface-mediated discharge mechanisms have been less studied, which is a focus of the present work.

Herein, the effects of the solvation properties of glyme-ether electrolytes and the nature of the carbon cathodes are probed to understand the influence of the cathode/aprotic electrolyte interfaces on product formation and cell performance. Three types of carbon cathodes are considered (Figure S1): Ketjen black (K.B.) carbon, Vulcan XC-72 carbon, and the commercial binder-free gas diffusion layer (GDL), which is used as a benchmark cathode due to its wide use. Type Two ether-based electrolyte solvents (DEGDME and TEGDME) with different solvation properties and chain lengths are investigated. The nature of the carbon cathode/aprotic solvent interface and the discharge mechanism for product formation are linked to the reported cell performance and stability.

The electrochemical performance of Na-O₂ cells with the short-chain electrolyte solvent, DEGDME, and varying carbon cathodes is initially probed to (i) benchmark the performance

ACS Energy Letters http://pubs.acs.org/journal/aelccp Letter

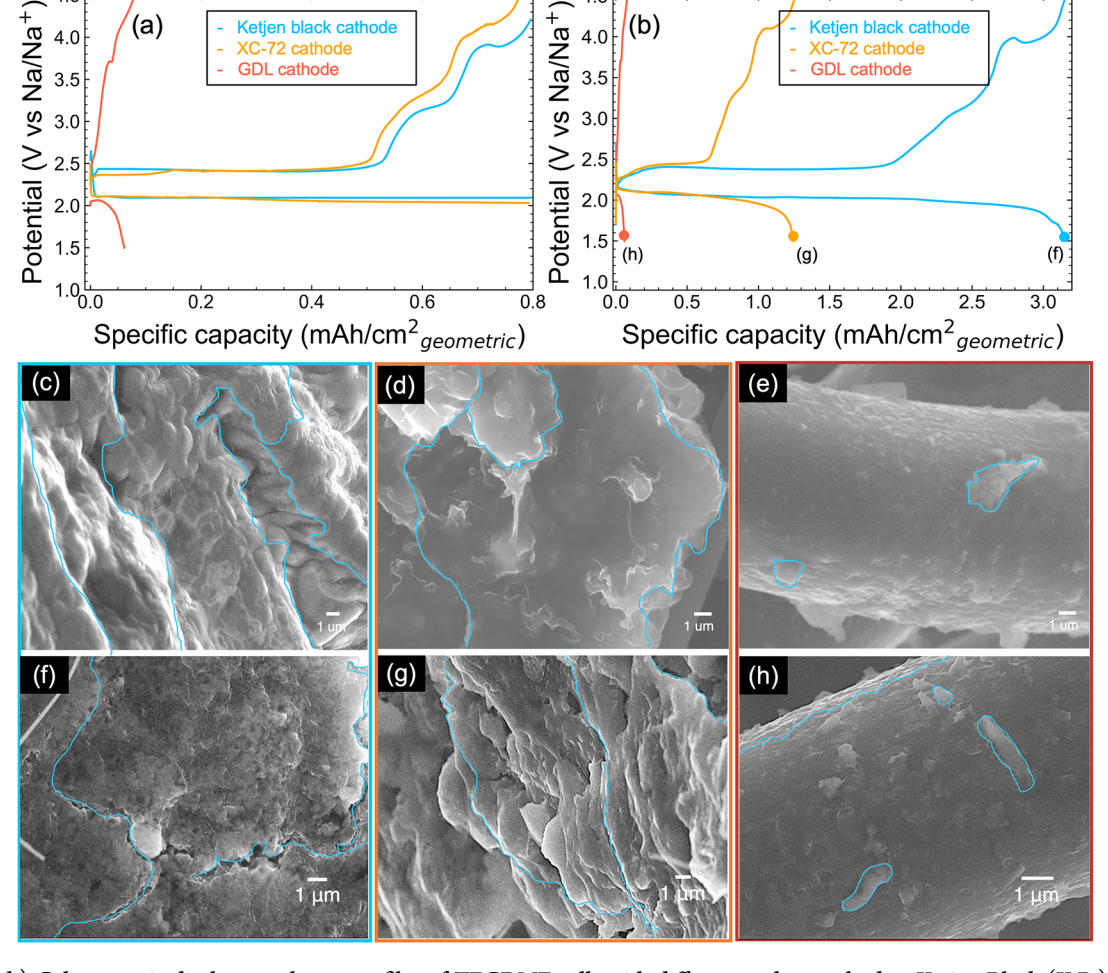


Figure 2. (a, b) Galvanostatic discharge-charge profiles of TEGDME cells with different carbon cathodes: Ketjen Black (K.B.) (blue), XC-72 (orange), and GDL (red), for a limited capacity of $0.79 \text{ mAh/cm}^2_{\text{geometric}}$ and full capacity, respectively, in a potential window of 1.5-4.5 V, at a current density of $80 \ \mu\text{A/cm}^2$. (c-e) SEM images post limited discharge for cells with K.B., XC-72, and GDL carbon cathodes, respectively. (f-h) SEM images post full discharge for cells with K.B., XC-72, and GDL carbon cathodes, respectively.

of the cells reported in this work, and (ii) determine the effects on the cell performance due to variations in the carbon cathode at the interface with DEGDME. Figure 1a,b shows the electrochemical performance of DEGDME cells with three different carbon cathodes (K.B., XC-72, and GDL) for limited (0.79 mAh/cm²_{geometric}) and full discharge capacity, respectively. For all these cells, a steady discharge potential of approximately 2 V vs Na/Na⁺ is observed during limited discharge (Figure 1a). Eventually, the cell potential drops to a cutoff limit of 1.5 V vs Na/Na⁺ (Figure 1b). As detailed in the Figure S2, Page S6 in the Supporting Information, the geometric area of the cathodes is used to normalize the cell capacity based on (i) standard practices as reported, 2,11,23,24,26 and (ii) the fact that it is a common parameter among all three carbon cathodes considered. We observe that the use of different carbon cathodes yields modest differences in the full discharge capacities (Figure 1b), which are much smaller than the differences in the BET (Brunauer-Emmett-Teller) surface area of the carbons (K.B. > XC-72 \gg GDL, Table S1).

X-ray diffraction (XRD) is employed to characterize the crystalline discharge products formed as a function of the carbon cathode post limited (Figure S3) and full discharge (Figure S4). In all cases, we observe a dominant XRD peak at a 2θ angle of approximately 32.7° . The simulated diffraction

patterns of the bulk structures from density functional theory (DFT) calculations suggest that the measured XRD patterns correspond to a pyrite NaO2 bulk structure (Figure S5). This analysis shows that varying the carbon cathode has minimal effect on the bulk structure of the crystalline discharge species, consistent with the literature.^{22,27} Post limited discharge SEM analysis shows pyrite NaO2 species with well-defined cubic structures (Figure 1c-e). However, post full discharge SEM shows structures that are distorted and physically larger than the limited discharge case (Figures 1f-h). The observed cubic structures are consistent with the reported solution-mediated discharge mechanism for DEGDME cells. 11,22,25 Interestingly, NaO₂ species are also observed on the glass-fiber separator, independent of the carbon cathode used (Figures S6 and S7), consistent with the chemical deposition of solvated Na+-O2agglomerates from solution onto a solid surface in a solutionmediated discharge process.

Significant differences are observed during charge between DEGDME cells discharged at limited and full capacities (Figure 1a,b). The limited-capacity charge behavior exhibits an initial plateau at 2.5 V vs Na/Na⁺ that lasts approximately 50% of the charge capacity, followed by a step increase in the charge potential (>3 V vs Na/Na⁺) for all three cathodes. The increase in the charge potential suggests the formation of

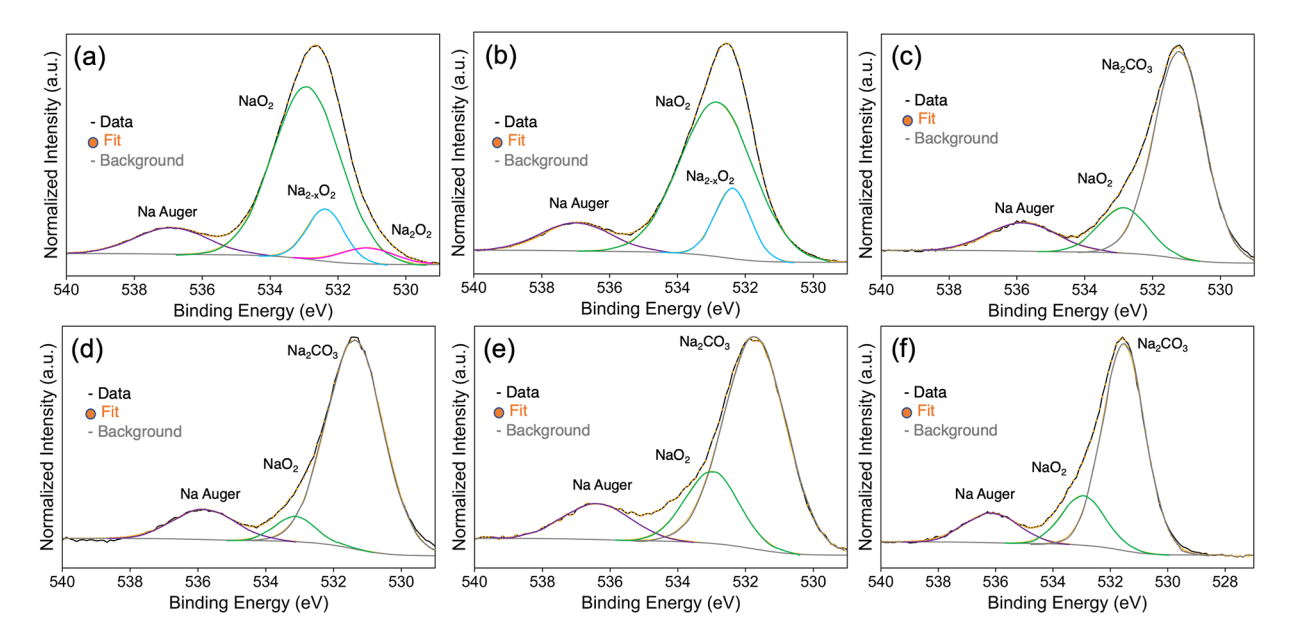


Figure 3. Fitted high-resolution O 1s spectra of the (a) K.B. cathode, (b) XC-72 cathode, and (c) GDL cathode of TEGDME cells, respectively, after limited discharge capacity studies. Fitted high-resolution O 1s spectra of the (d) K.B. cathode, (e) XC-72 cathode, and (f) GDL cathode of TEGDME cells, respectively, post full discharge capacity studies.

additional discharge product phases¹⁴ beyond the crystalline pyrite NaO2 detected by XRD. To characterize these species, we have used high-resolution XPS analysis of the C 1s and O 1s core binding states of the discharged cathodes (Figures S8 and S9, respectively). These measurements were conducted ex situ; however, the exposure of the cathodes to air was minimal (Methods in the Supporting Information). Post limited discharge, the XPS analysis of the O 1s core binding state suggests the formation of mainly Na-oxide species (NaO₂, ²⁸ $Na_{2-x}O_2$, and Na_2O_2 , Figure S9a-c). Post full discharge, a mix of NaO₂ and Na₂CO₃ phases is observed (Figure S9d-f). The formation of Na₂CO₃ is related to electrolyte degradation.³¹ Unlike the limited capacity studies, the fullcapacity charge behavior exhibits an initial charge plateau (Figure 1b) that is short-lived, at less than 10% of the full discharge capacity for all three cells. Upon further charging, the cell potential exhibits significant fluctuations (Figure 1b) above 3 V vs Na/Na⁺, indicative of cell failure. These fluctuations arise from dendrite formation, ^{32,33} as corroborated by SEM showing needle-like structures puncturing the separator (Figure 1i–k).

To determine changes induced by the nature (solvation properties) of the electrolyte solvent, studies similar to the case of DEGDME are performed using a long-chain glyme-ether solvent, such as TEGDME. Figure 2a,b shows the galvanostatic discharge—charge profiles of TEGDME cells with varying carbon cathodes for limited and full discharge, respectively. Unlike DEGDME cells, Figure 2b displays a dependence of the discharge capacity on the carbon cathodes used, which scales linearly with the BET surface area of the carbon (K.B. > XC-72 >> GDL).

In addition to surface area effects, differences in the surface structure and functionality of the carbon surface (Figure S10) might also impact the observed discharge behavior and require further studies to interrogate, which are beyond the scope of this study. XRD analysis of the cathodes after limited and full discharge (Figures S11 and S12) shows a dominant peak at a 2θ angle of \sim 32.7° for the K.B. and XC-72 cells, corresponding

to pyrite NaO₂. For GDL, an indiscernible XRD pattern (Figure S13) arises due to low discharge capacity. ¹¹ SEM imaging of the cathodes post limited and full discharge (Figure 2c-h) shows film-like morphologies of the discharge products, a significant deviation from the cube structures observed for DEGDME cells. ¹¹ The 2-D growth of the discharge products along the carbon surface in TEGDME cells indicates a surface-mediated discharge product formation.

Charge energetics post limited and full discharge for the high-surface-area carbon cathodes (K.B. and XC-72) are very similar (Figure 2a,b), unlike in the case of DEGDME cells, wherein there is an initial charge plateau at 2.4 V vs Na/Na⁺ that lasts $\sim\!60\%$ of the charge capacity, beyond which a step increase is observed (>3 V vs Na/Na⁺). As discussed above, the initial plateau corresponds to the decomposition of the NaO₂, while the increase in the charge potential corresponds to the decomposition of other species. In the case of the GDL cell, a rapid increase in the charge potential that reaches a cutoff value of 4.5 V vs Na/Na⁺ is observed.

The fitted O 1s high-resolution XPS spectra (Figure 3a,b) for K.B. and XC-72 cathodes post limited discharge suggest the presence of NaO₂ (532.9 eV)²⁸ and deficient superoxide species $(Na_{2-x}O_2, 0 < x < 1)$ (532.3 eV).²⁹ However, for the GDL cathode (Figure 3c), formation of the Na₂CO₃ phase (531.5 eV)³⁰ in addition to NaO₂ (532.9 eV) is observed. Na₂CO₃ is also observed after full discharge on all three carbon cathodes (Figure 3d-f), along with the NaO2 phase from the deconvolution of the O 1s spectra. This is further confirmed by the analysis of the C 1s core binding state, which shows a peak at 288.4 eV (Figure S14c-f) assigned to the C=O stretch, 25 indicating the formation of carbonate species which are absent for the case of K.B and XC-72 cathodes post limited discharge (Figure S14a,b). Undissociated remanent films (Figure S15a,c) of Na-O₂ and Na₂CO₃ (Figure S15d-f) species are also observed post charge. Unlike the case of DEGDME cells, no dendrite formation is observed (Figure S16), potentially due to the strong TEGDME-solute interactions, limiting the transport

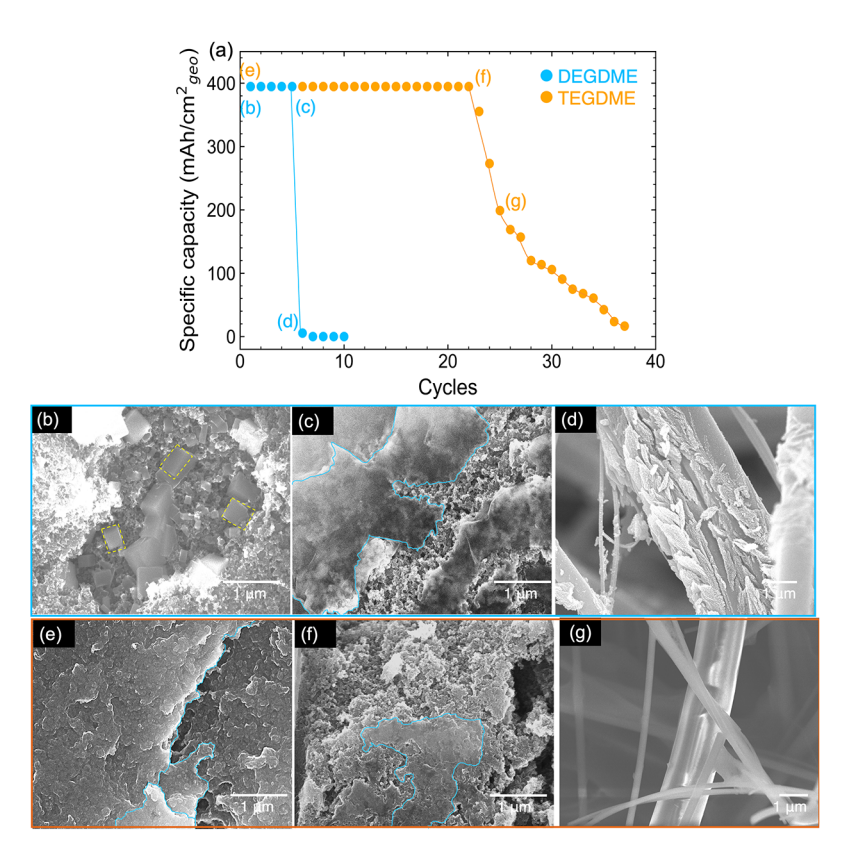
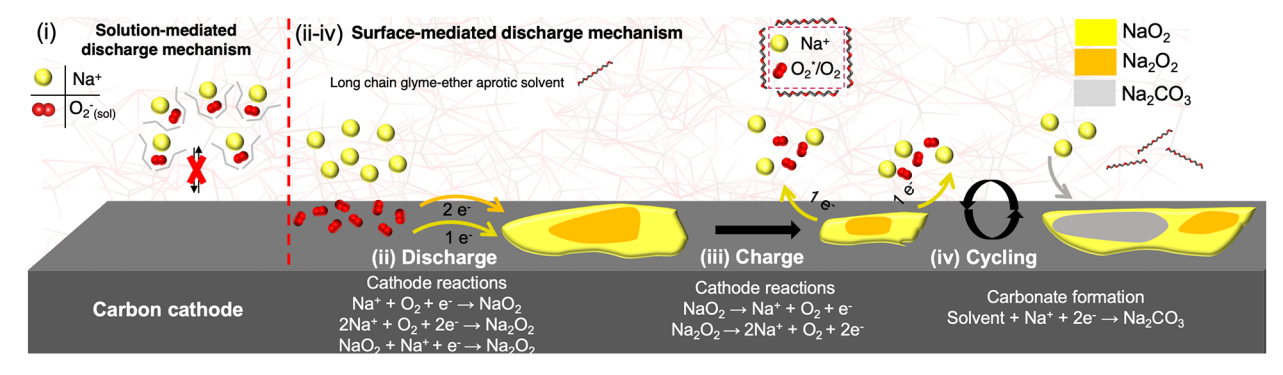


Figure 4. (a) Cycling performance of DEGDME-K.B. and TEGDME-K.B. $Na-O_2$ cells for a discharge capacity of 0.395 mAh/cm² geometric (blue and orange plots, respectively) within a cutoff limit of 1.5–4.5 V vs Na/Na^+ (Figure S19c shows reproducibility studies). SEM images of the cathode post 1st (b) and 5th discharge stages (c) and the separator post 5th charge stage (d) for the DEGDME-K.B. cell. SEM images of the cathode after the 1st (e) and 22nd discharge stages (f), and the separator after the 25th charge stage (g) for the TEGDME-K.B. cell.

Scheme 1. Illustration of Discharge Processes at a Carbon/Long-Chain Glyme-Ether Aprotic Solvent (i.e., TEGDME) Interface^a



"Solution-mediated discharge pathway (i) is not energetically favorable at the carbon cathode/TEGDME interface due to high barriers for solvation of the Na⁺-O₂⁻ species in TEGDME. A cathode surface-mediated mechanism dominates the discharge process. In a surface-mediated pathway, a pristine cathode serves as the active surface for oxygen adsorption followed by (ii) 1e- and/or 2e-transfer processes leading to the formation of NaO₂ or Na₂O₂ films, respectively, during discharge, as supported by our XRD and XPS studies (e.g., Figures S11 and S12 and Figure 3, respectively). Upon charge (iii), the NaO₂ films are fully decomposed, while remanent Na₂O₂ films are observed on the cathode surface, as evidenced by XPS (e.g., Figure S15e), due to the much higher overpotential barrier required to dissociate this product. (iv) Subsequent cycling of the cell results in the accumulation of the side products at the carbon/TEGDME interface, such as Na₂O₂ and Na₂CO₃, as indicated by XPS and SEM analysis (e.g., Figures S20e and S22, respectively).

of solvated oxygen species to the anode and suppressing dendrite formation.³⁴

Cell cyclability is probed via galvanostatic cyclic discharge—charge experiments at a limited capacity of 0.395 mAh/cm²_{geometric} (shallow cycling). K.B. carbon is kept consistent in these studies, since it is the best-performing cathode at the interface with both solvents. Figure 4a shows that the

DEGDME-K.B. cell exhibits a stable performance up to cycle 5 followed by an abrupt decrease in the discharge capacity. In contrast, the TEGDME-K.B. cell exhibits stable performance for up to 22 cycles, followed by a gradual decline in the discharge capacity (Figure 4a, orange). Post characterization of the DEGDME-K.B. cell (Figure 4b) shows the formation of cubes after the first cycle identified as crystalline pyrite NaO₂

via XRD (Figure S17a). However, after the fifth discharge cycle, only film-like structures are observed (Figure 4c). The identified discharge products from XPS are listed in Table S2 (Figures S18 and S20). Post first cycle, for the DEGDME-K.B. cell at a discharge potential of \sim 2 V vs Na/Na $^+$, Na $^-$ O₂ species (NaO₂ and Na₂O₂) (Figure S18d) are mainly identified. Further cycling (5th discharge) leads to the formation of Na₂CO₃ as the major phase in the near-surface region (Figure S18e). If we consider the fifth charge cycle of the cell, the charge potential rapidly increases beyond \sim 3 V vs Na/Na $^+$ and starts fluctuating (Figure S19a). When the separator of the cell is characterized post 5th charge, we observe needle-like structures consistent with dendrite formation (Figure 4d).

The TEGDME-K.B. cell, exhibits 5-fold increase in stable cycling compared to the DEGDME-K.B. cell. . Film-like structures are observed throughout the cycling study (Figure 3e,f). Pyrite NaO2 is the major crystalline phase, as corroborated by XRD until the 22nd discharge stage (Figure S17b), beyond which no discernible crystalline phase is observed. XPS analysis shows Na-O2 species form post first discharge (Table S2 and Figure S20d). Post 22nd cycle, we observe the formation of Na₂CO₃ in addition to Na-O₂ species (Table S2 and Figure S20e). After the 22nd discharge, the capacity gradually decreases, discharge-charge overpotentials increase (Figure S19b), and the undesired discharge products (i.e., Na₂CO₃) dominate the cathode surface as corroborated by the deconvoluted high-resolution C 1s and O 1s XPS spectra (Figure S20c,f, respectively). The absence of dendrites (Figure 4g) suggests that the accumulation of these undesired side products upon further cycling passivates the cathode surface, eventually causing cell failure.

In aggregate, our results suggest that the discharge mechanism, the energetics of discharge-charge, and the cyclability of Na-O2 batteries are significantly influenced by the nature of the electrode/electrolyte interfaces. We find that independent of the extent of discharge or the nature of the carbon cathode, film-like products form in TEGDME cells, distinct from the thermodynamically stable cubic structures observed in DEGDME cells (Figures 2c-h and 1c-h, respectively). This difference stems from the cathode-surfacemediated discharge process in TEGDME cells as opposed to the solution-mediated discharge in DEGDME cells. Scheme 1 illustrates the proposed steps involved in the surface-mediated mechanism at the carbon cathode/TEGDME interfaces based on our reported observations. In this mechanism, the pristine cathode serves as the active surface for oxygen adsorption followed by 1- and/or 2-electron-transfer processes leading to the formation of NaO2 or Na2O2 films 16 during discharge, respectively, as supported by our XRD and XPS studies (e.g., Figures S11 and S12 and Figure 3, respectively). Thus, oxygen adsorption on the cathode surface plays an important role in this process, consistent with the observed changes in the TEGDME cell performance (e.g., Figure 2b) resulting from variations in the nature of the carbon cathode, which impacts the quantity and nature of oxygen adsorption sites. Upon charge, remanent traces of Na-O2 and Na2CO3 films are observed on the carbon cathode surface, as evidenced by XPS (e.g., Figure S15e,f), that eventually passivate the surface during cycling, leading to cell failure.

Differences in the deactivation mechanisms of these cells are observed, arising from differences in the solvation properties of the respective electrolyte solvents. In the case of DEGDME cells, deactivation is primarily induced by the formation of

dendrites (Figure S21). This is consistent with literature reports which show that O₂⁻ crossover³⁴ in DEGDME cells leads to parasitic reactions and destabilization of the anode/ electrolyte interface (SEI), 32,35 promoting dendrite formation. Strategies to mitigate dendrite formation in DEGDME cells include the use of membranes or coatings to protect the anode. 34,36 Conversely, TEGDME exhibits strong interactions with the Na salt, inducing a high barrier for interaction of the O₂ ions with the electrolyte molecules preventing their crossover to the anode, limiting dendrite formation. As a result, The reported results show that TEGDME cells deactivate due to the formation of undesired side products (Scheme 1-iv), which gradually passivate the carbon cathode surface. Given the surface-mediated nature of discharge in TEGDME cells, tuning the cathode surface can be used to improve their overall efficiency and cyclability.

ASSOCIATED CONTENT

Supporting Information

The Supporting Information is available free of charge at https://pubs.acs.org/doi/10.1021/acsenergylett.3c01664.

Details of experimental and computational procedures, SEM images of as-fabricated carbon cathodes and separator, comparison of the effects of different normalization methods on the interpretation of the observed discharge-charge behavior between the K.B. and the XC-72 carbon cathodes, details of the physical aspects of the commercial carbon nanoparticles, XRD patterns of the DEGDME cells post limited and full discharge, simulated XRD patterns using DFT for the pyrite and marcasite phases, SEM images of the separator post discharge, high-resolution C 1s and O 1s XPS scans for the DEGDME cells post limited and full discharge, O 1s XPS scans for as-prepared cathodes, XRD patterns for the TEGDME cells post limited and full discharge, highresolution C 1s and O 1s XPS scans for the TEGDME cells post limited and full discharge, XPS analysis post charge for the TEGDME cell, XRD and XPS analysis of cells as a function of cycling, discharge-charge energetics as a function of cycling, summary of identified species using high resolution O 1s spectra, cycling performance of DEGDME and TEGDME cells along with error bars for stability, characterizing the anode during charge for the DEGDME and TEGDME cell, ex situ SEM imaging to show remanent film-like structures for a TEGDME cell post 22nd and 25th cycles (PDF)

■ AUTHOR INFORMATION

Corresponding Authors

Jeffrey Greeley — Davidson School of Chemical Engineering, Purdue University, West Lafayette, Indiana 47907, United States; oorcid.org/0000-0001-8469-1715;

Email: jgreeley@purdue.edu

Eranda Nikolla — Department of Chemical Engineering, University of Michigan, Ann Arbor, Michigan 48109, United States; Orcid.org/0000-0002-8172-884X;

Email: erandan@umich.edu

Authors

Kunal Kalpesh Velinkar — Department of Chemical Engineering, University of Michigan, Ann Arbor, Michigan 48109, United States Alex Von Gunten – Davidson School of Chemical Engineering, Purdue University, West Lafayette, Indiana 47907, United States

Complete contact information is available at: https://pubs.acs.org/10.1021/acsenergylett.3c01664

Author Contributions

The manuscript was written through the contributions of all authors. All authors have given approval to the final version of the manuscript.

Notes

The authors declare no competing financial interest.

■ ACKNOWLEDGMENTS

We gratefully acknowledge funding from the United States National Science Foundation under award numbers CBET-2312634/1935581 and CBET-1935645. In addition, A.V.G. and J.G. gratefully acknowledge the computational resources from the National Energy Research Scientific Computing Center and the resources from Purdue University Research Computing.

REFERENCES

- (1) Hartmann, P.; Bender, C. L.; Vračar, M.; Dürr, A. K.; Garsuch, A.; Janek, J.; Adelhelm, P. A Rechargeable Room-Temperature Sodium Superoxide (NaO2) Battery. *Nat. Mater.* **2013**, *12* (3), 228–232.
- (2) Morasch, R.; Kwabi, D. G.; Tulodziecki, M.; Risch, M.; Zhang, S.; Shao-Horn, Y. Insights into Electrochemical Oxidation of NaO 2 in Na-O 2 Batteries via Rotating Ring Disk and Spectroscopic Measurements. ACS Appl. Mater. Interfaces. 2017, 9 (5), 4374–4381.
- (3) Kwak, W.-J.; Rosy; Sharon, D.; Xia, C.; Kim, H.; Johnson, L. R.; Bruce, P. G.; Nazar, L. F.; Sun, Y.-K.; Frimer, A. A.; Noked, M.; Freunberger, S. A.; Aurbach, D. Lithium-Oxygen Batteries and Related Systems: Potential, Status, and Future. *Chem. Rev.* **2020**, 120 (14), 6626–6683.
- (4) Lu, J.; Jung Lee, Y.; Luo, X.; Chun Lau, K.; Asadi, M.; Wang, H.-H.; Brombosz, S.; Wen, J.; Zhai, D.; Chen, Z.; Miller, D. J.; Sub Jeong, Y.; Park, J.-B.; Zak Fang, Z.; Kumar, B.; Salehi-Khojin, A.; Sun, Y.-K.; Curtiss, L. A.; Amine, K. A Lithium-Oxygen Battery Based on Lithium Superoxide. *Nature.* **2016**, *529* (7586), 377–382.
- (5) Bi, X.; Wang, R.; Amine, K.; Lu, J. A Critical Review on Superoxide-Based Sodium-Oxygen Batteries. *Small Methods.* **2019**, 3 (4), 1800247.
- (6) Yadegari, H.; Sun, Q.; Sun, X. Sodium-Oxygen Batteries: A Comparative Review from Chemical and Electrochemical Fundamentals to Future Perspective. *Adv. Mater.* **2016**, *28* (33), 7065–7093.
- (7) Wanger, T. C. The Lithium Future-Resources, Recycling, and the Environment. *Conserv Lett.* **2011**, *4* (3), 202–206.
- (8) Samira, S.; Deshpande, S.; Roberts, C. A.; Nacy, A. M.; Kubal, J.; Matesić, K.; Oesterling, O.; Greeley, J.; Nikolla, E. Nonprecious Metal Catalysts for Tuning Discharge Product Distribution at Solid-Solid Interfaces of Aprotic Li-O2 Batteries. *Chem. Mater.* **2019**, *31* (18), 7300–7310.
- (9) Nacy, A.; Ma, X.; Nikolla, E. Nanostructured Nickelate Oxides as Efficient and Stable Cathode Electrocatalysts for Li-O2 Batteries. *Top Catal.* **2015**, *58*, *513*–*521*.
- (10) Kang, S.; Mo, Y.; Ong, S. P.; Ceder, G. Nanoscale Stabilization of Sodium Oxides: Implications for Na-O $_2$ Batteries. *Nano Lett.* **2014**, 14 (2), 1016–1020.
- (11) Lutz, L.; Yin, W.; Grimaud, A.; Alves Dalla Corte, D.; Tang, M.; Johnson, L.; Azaceta, E.; Sarou-Kanian, V.; Naylor, A. J.; Hamad, S.; Anta, J. A.; Salager, E.; Tena-Zaera, R.; Bruce, P. G.; Tarascon, J.-M. High Capacity Na-O2 Batteries: Key Parameters for Solution-Mediated Discharge. *J. Phys. Chem. C* 2016, 120 (36), 20068–20076.

- (12) Aldous, I. M.; Hardwick, L. J. Solvent-Mediated Control of the Electrochemical Discharge Products of Non-Aqueous Sodium-Oxygen Electrochemistry. *Angew. Chem., Int. Ed.* **2016**, *55* (29), 8254–8257.
- (13) Dilimon, V. S.; Hwang, C.; Cho, Y.-G.; Yang, J.; Lim, H.-D.; Kang, K.; Kang, S. J.; Song, H.-K. Superoxide Stability for Reversible Na-O2 Electrochemistry. *Sci. Rep.* **2017**, *7* (1), 17635.
- (14) Bender, C. L.; Schröder, D.; Pinedo, R.; Adelhelm, P.; Janek, J. One- or Two-Electron Transfer? The Ambiguous Nature of the Discharge Products in Sodium-Oxygen Batteries. *Angew. Chem., Int. Ed.* **2016**, *55* (15), 4640–4649.
- (15) Kim, J.; Park, H.; Lee, B.; Seong, W. M.; Lim, H.-D.; Bae, Y.; Kim, H.; Kim, W. K.; Ryu, K. H.; Kang, K. Dissolution and Ionization of Sodium Superoxide in Sodium-Oxygen Batteries. *Nat. Commun.* **2016**, *7* (1), 10670.
- (16) Von Gunten, A.; Velinkar, K.; Nikolla, E.; Greeley, J. Elucidation of Parasitic Reaction Mechanisms at Interfaces in Na-O 2 Batteries. *Chem. Mater.* **2023**, *35*, 5945.
- (17) Zhang, Y.; Ortiz-Vitoriano, N.; Acebedo, B.; O'Dell, L.; MacFarlane, D. R.; Rojo, T.; Forsyth, M.; Howlett, P. C.; Pozo-Gonzalo, C. Elucidating the Impact of Sodium Salt Concentration on the Cathode-Electrolyte Interface of Na-Air Batteries. *Angew. Chem., Int. Ed.* **2018**, 122 (27), 15276–15286.
- (18) He, M.; Lau, K. C.; Ren, X.; Xiao, N.; McCulloch, W. D.; Curtiss, L. A.; Wu, Y. Concentrated Electrolyte for the Sodium-Oxygen Battery: Solvation Structure and Improved Cycle Life. *Angew. Chem., Int. Ed.* **2016**, *55* (49), 15310–15314.
- (19) Qin, B.; Chan, K.-Y.; Li, C.-Y. V. Studies of Superoxide Degradation Kinetics and Electrolyte Management for a Reversible NaO ₂ Battery. ACS Sustain Chem. Eng. 2020, 8 (11), 4317–4324.
- (20) Tatara, R.; Leverick, G. M.; Feng, S.; Wan, S.; Terada, S.; Dokko, K.; Watanabe, M.; Shao-Horn, Y. Tuning NaO2 Cube Sizes by Controlling Na+ and Solvent Activity in Na-O2 Batteries. *J. Phys. Chem. C* 2018, 122 (32), 18316–18328.
- (21) Hartmann, P.; Grübl, D.; Sommer, H.; Janek, J.; Bessler, W. G.; Adelhelm, P. Pressure Dynamics in Metal-Oxygen (Metal-Air) Batteries: A Case Study on Sodium Superoxide Cells. *J. Phys. Chem.* C **2014**, *118* (3), 1461–1471.
- (22) Bender, C. L.; Hartmann, P.; Vračar, M.; Adelhelm, P.; Janek, J. On the Thermodynamics, the Role of the Carbon Cathode, and the Cycle Life of the Sodium Superoxide (NaO₂) Battery. *Adv. Eng. Mater.* **2014**, *4* (12), 1301863.
- (23) Lutz, L.; Corte, D. A. D.; Chen, Y.; Batuk, D.; Johnson, L. R.; Abakumov, A.; Yate, L.; Azaceta, E.; Bruce, P. G.; Tarascon, J. M.; Grimaud, A. The Role of the Electrode Surface in Na-Air Batteries: Insights in Electrochemical Product Formation and Chemical Growth of NaO2. *Adv. Eng. Mater.* **2018**, *8*, 4.
- (24) Lutz, L.; Alves Dalla Corte, D.; Tang, M.; Salager, E.; Deschamps, M.; Grimaud, A.; Johnson, L.; Bruce, P. G.; Tarascon, J.-M. Role of Electrolyte Anions in the Na-O ₂ Battery: Implications for NaO ₂ Solvation and the Stability of the Sodium Solid Electrolyte Interphase in Glyme Ethers. *Chem. Mater.* **2017**, *29* (14), 6066–6075.
- (25) Hartmann, P.; Bender, C. L.; Sann, J.; Dürr, A. K.; Jansen, M.; Janek, J.; Adelhelm, P. A Comprehensive Study on the Cell Chemistry of the Sodium Superoxide (NaO2) Battery. *Phys. Chem. Chem. Phys.* **2013**, *15* (28), 11661.
- (26) Enterría, M.; Mysyk, R.; Medinilla, L.; Villar-Rodil, S.; Paredes, J. I.; Rincón, I.; Fernández-Carretero, F. J.; Gómez, K.; del Amo, J. M. L.; Ortiz-Vitoriano, N. Increasing the Efficiency and Cycle Life of Na-O2 Batteries Based on Graphene Cathodes with Heteroatom Doping. *Electrochim. Acta* 2023, 445, 142056.
- (27) Enterría, M.; Reynaud, M.; Paredes, J. I.; Medinilla, L.; Younesi, R.; Ortiz-Vitoriano, N. Driving the Sodium-Oxygen Battery Chemistry towards the Efficient Formation of Discharge Products: The Importance of Sodium Superoxide Quantification. *J. Eng. Chem.* **2022**, *68*, 709–720.
- (28) Jovanov, Z. P.; Lutz, L.; Lozano, J. G.; Holc, C.; Gao, X.; Grimaud, A.; Tarascon, J.; Chen, Y.; Johnson, L. R.; Bruce, P. G. Competitive Oxygen Reduction Pathways to Superoxide and Peroxide

- during Sodium-Oxygen Battery Discharge. Batter Supercaps. 2022, 5, 9.
- (29) Yadegari, H.; Li, Y.; Banis, M. N.; Li, X.; Wang, B.; Sun, Q.; Li, R.; Sham, T.-K.; Cui, X.; Sun, X. On Rechargeability and Reaction Kinetics of Sodium-Air Batteries. *Energy Environ. Sci.* **2014**, *7* (11), 3747–3757.
- (30) Hammond, J. S.; Holubka, J. W.; deVries, J. E.; Dickie, R. A. The Application of X-Ray Photo-Electron Spectroscopy to a Study of Interfacial Composition in Corrosion-Induced Paint de-Adhesion. *Corros. Sci.* 1981, 21 (3), 239–253.
- (31) Lutz, L.; Dachraoui, W.; Demortière, A.; Johnson, L. R.; Bruce, P. G.; Grimaud, A.; Tarascon, J.-M. Operando Monitoring of the Solution-Mediated Discharge and Charge Processes in a Na-O ₂ Battery Using Liquid-Electrochemical Transmission Electron Microscopy. *Nano Lett.* **2018**, *18* (2), 1280–1289.
- (32) Medenbach, L.; Bender, C. L.; Haas, R.; Mogwitz, B.; Pompe, C.; Adelhelm, P.; Schröder, D.; Janek, J. Origins of Dendrite Formation in Sodium-Oxygen Batteries and Possible Countermeasures. *Eng. Technol.* **2017**, *5* (12), 2265–2274.
- (33) Lin, X.; Sun, Q.; Yadegari, H.; Yang, X.; Zhao, Y.; Wang, C.; Liang, J.; Koo, A.; Li, R.; Sun, X. On the Cycling Performance of Na-O ₂ Cells: Revealing the Impact of the Superoxide Crossover toward the Metallic Na Electrode. *Adv. Funct. Mater.* **2018**, 28 (35), 1801904.
- (34) Lin, X.; Sun, F.; Sun, Q.; Wang, S.; Luo, J.; Zhao, C.; Yang, X.; Zhao, Y.; Wang, C.; Li, R.; Sun, X. O ₂ /O ₂ ⁻ Crossover- and Dendrite-Free Hybrid Solid-State Na-O ₂ Batteries. *Chem. Mater.* **2019**, *31* (21), 9024–9031.
- (35) Zhao, S.; Qin, B.; Chan, K. Y.; Li, C. Y. V.; Li, F. Recent Development of Aprotic Na-O2 Batteries. *Batter. Supercaps. Wiley-VCH Verlag* **2019**, *2*, 725–742.
- (36) Zhao, S.; Wang, C.; Du, D.; Li, L.; Chou, S.; Li, F.; Chen, J. Bifunctional Effects of Cation Additive on Na-O ₂ Batteries. *Angew. Chem., Int. Ed.* **2021**, 133 (6), 3242–3248.